Atmos. Chem. Phys., 12, 3165–3179, 2012
www.atmos-chem-phys.net/12/3165/2012/
doi:10.5194/acp-12-3165-2012

Atmospheric Chemistry and Physics

Particle mass yield from β-caryophyllene ozonolysis

Q. Chen[1], Y. L. Li[1,2], K. A. McKinney[3], M. Kuwata[1], and S. T. Martin[1,4]

[1]School of Engineering and Applied Sciences, Harvard University, Cambridge, Massachusetts, USA
[2]Division of Environment, Hong Kong University of Science and Technology, Hong Kong, China
[3]Department of Chemistry, Amherst College, Amherst, Massachusetts, USA
[4]Department of Earth and Planetary Sciences, Harvard University, Cambridge, Massachusetts, USA

Correspondence to: S. T. Martin (scot_martin@harvard.edu)

Received: 26 October 2011 – Published in Atmos. Chem. Phys. Discuss.: 14 November 2011
Revised: 29 February 2012 – Accepted: 12 March 2012 – Published: 3 April 2012

Abstract. The influence of second-generation products on the particle mass yield of β-caryophyllene ozonolysis was systematically tested and quantified. The approach was to vary the relative concentrations of first- and second-generation products by adjusting the concentration of ozone while observing changes in particle mass yield. For all wall-loss corrected organic particle mass concentrations M_{org} of this study ($0.5 < M_{org} < 230\,\mu g\,m^{-3}$), the data show that the particle-phase organic material was composed for the most part of second-generation products. For $0.5 < M_{org} < 10\,\mu g\,m^{-3}$, a range which overlaps with atmospheric concentrations, the particle mass yield was 10 to 20 % and was not sensitive to ozone exposure, implying that the constituent molecules were rapidly produced at all investigated ozone exposures. In contrast, for $M_{org} > 10\,\mu g\,m^{-3}$ the particle mass yield increased to as high as 70 % for the ultimate yield corresponding to the greatest ozone exposures. These differing dependencies on ozone exposure under different regimes of M_{org} are explained by a combination of the ozonolysis lifetimes of the first-generation products and the volatility distribution of the resulting second-generation products. First-generation products that have short lifetimes produce low-volatility second-generation products whereas first-generation products that have long lifetimes produce high-volatility second-generation products. The ultimate particle mass yield was defined by mass-based stoichiometric yields α_i of $\alpha_0 = 0.17 \pm 0.05$, $\alpha_1 = 0.11 \pm 0.17$, and $\alpha_2 = 1.03 \pm 0.30$ for corresponding saturation concentrations of 1, 10, and $100\,\mu g\,m^{-3}$. Terms α_0 and α_1 had low sensitivity to the investigated range of ozone exposure whereas term α_2 increased from 0.32 ± 0.13 to 1.03 ± 0.30 as the ozone exposure was increased. These findings potentially allow for simplified yet accurate parameterizations in air quality and climate models that seek to represent the ozonolysis particle mass yields of certain classes of biogenic compounds.

1 Introduction

Sesquiterpene emissions have been estimated as 10–30 % of those of monoterpenes (Helmig et al., 2007; Sakulyanontvittaya et al., 2008a). Because of their fast ozonolysis reactivity and their tendency to form low-volatility products, sesquiterpenes ($C_{15}H_{24}$) are important precursor molecules to secondary organic material (SOM) (Hoffmann et al., 1997; Jaoui and Kamens, 2003; Jaoui et al., 2003). For instance, β-caryophyllinic acid, which is an ozonolysis product of the sesquiterpene β-caryophyllene, has been measured at substantial concentrations for ambient particles in environments as diverse as the tropics and the arctic (Jaoui et al., 2007; Hu et al., 2008; Fu et al., 2009). For typical concentrations of tropospheric oxidants, the lifetimes of sesquiterpenes are about 2 min for the reaction with ozone, 2–3 min for the reaction with nitrate radicals at night, and 30–40 min for the reaction with hydroxyl radicals in the day (Shu and Atkinson, 1995). Sesquiterpene emissions usually occur during the day (Helmig et al., 2007). Reaction with ozone is therefore regarded as the dominant degradation pathway of many sesquiterpenes in the atmosphere (Atkinson and Arey, 2003).

As one of the most atmospherically prevalent sesquiterpenes, β-caryophyllene has been studied extensively in the laboratory. The reported particle mass yields associated with its oxidation range from 6–62 % for dark ozonolysis and from 37–125 % for photooxidation (Grosjean et al., 1993;

Hoffmann et al., 1997; Griffin et al., 1999; Jaoui et al., 2003; Lee et al., 2006a, b; Winterhalter et al., 2009) (Table 1). Particle mass yield Y is defined as the organic particle mass concentration ΔM_{org} that is produced divided by the mass concentration of the precursor volatile organic compound ΔVOC that is reacted (Odum et al., 1996): $Y \equiv \Delta M_{org}/\Delta VOC$. Yield depends to a first approximation on the volatility of the reaction products. An implication is that the relative tendency of molecules to partition from the gas phase to the particle phase (i.e., ΔM_{org}) depends on the extent of particle phase (i.e., M_{org}) that is present (Pankow, 1994a,b). Reaction conditions also influence yield by affecting the relative importance of competing kinetic pathways and hence the relative proportion of products of differing volatilities (Chan et al., 2007). Important experimental conditions include relative humidity, particle acidity, ozone concentration, and NO_x concentration (Ng et al., 2007; Offenberg et al., 2009; Winterhalter et al., 2009). Winterhalter et al. (2009), for example, demonstrated that the addition of gas-phase formic acid or water scavenged reactive Criegee intermediates and thereby influenced the concentration profile of the reaction products, ultimately leading to a doubling of the particle mass yield by β-caryophyllene ozonolysis. Offenberg et al. (2009) showed that increased particle acidity led to greater particle mass yields from β-caryophyllene photooxidation.

Among the several factors influencing particle mass yield from β-caryophyllene ozonolysis, the stoichiometric ratio of ozone to β-caryophyllene is an especially important regulator. β-caryophyllene has two double bonds, and the endocyclic bond is more reactive to ozone by two orders of magnitude than is the exocyclic bond (Nguyen et al., 2009; Winterhalter et al., 2009). Second-generation products are produced by ozonolysis of the remaining double bond of the first-generation products. The second-generation products typically have lower vapor pressures and hence greater thermodynamic tendencies to condense to the particle phase (Li et al., 2011). As a result, particle mass yield increases significantly in the case that sufficient ozone is present for first-generation products to continue oxidation. For instance, when injecting excess ozone, Ng et al. (2006) observed continued and rapid particle growth even after β-caryophyllene was completely consumed. This observation was explained by the production and gas-to-particle condensation of second-generation products.

In the atmosphere, concentrations of biogenic volatile organic compounds (BVOCs) are ultimately limited by their surface emissions and are normally less than 10 ppbv in forested environments (Helmig et al., 1998). By comparison, ozone concentrations range from 10 to 30 ppbv at background sites (Fiore et al., 2003) to over 100 ppbv for urban locations (Solomon et al., 2000). Moreover, the atmospheric concentration of ozone is continuously renewed by atmospheric production. The implication is that under most circumstances the ozone exposure in the atmosphere is in excess of the possible consumption by BVOCs, especially for sesquiterpenes. Few laboratory studies, however, have carried out experiments for conditions of excess ozone (i.e., ozone: β-caryophyllene > 2) (Table 1). As such, particle mass yield in the regime of second-generation dominance remains largely unknown, especially for conditions that overlap with atmospheric concentrations ($M_{org} < 10\,\mu g\,m^{-3}$).

Herein, experimental observations for the dark ozonolysis of β-caryophyllene (0.8–46 ppbv) under various conditions of excess ozone are reported. The qualitative molecular identification of the particle-phase products for these experiments and an associated discussion of their production mechanisms were presented in Li et al. (2011). An analysis of oxygen-to-carbon (O:C) and hydrogen-to-carbon (H:C) elemental ratios was presented in Chen et al. (2011) in a comparative study of isoprene, α-pinene, and β-caryophyllene. In relation to these two earlier reports, the focus of the present report is on second-generation products and their effects on particle mass yield.

2 Experimental

2.1 Experimental procedures and measurements

Experiments were carried out in the Harvard Environmental Chamber. Detailed descriptions of the chamber were previously published (Shilling et al., 2008; King et al., 2009). Compared to those reports, in this study a 0.13-mm (5-mil) thick PFA Teflon bag having a volume V of 4.7 m^3 was newly installed as a replacement for the previously described 0.05-mm (2-mil) PFA bag. As in the earlier studies, the bag served as a continuously mixed flow reactor (CMFR) (Kleindienst et al., 1999; Seinfeld et al., 2003). A flow Q of 22 l min^{-1} was used, corresponding to a mean residence time τ of 3.6 h, as calculated by $\tau = V/Q$. Temperature and relative humidity were held at 25 ± 1 °C and 40 ± 1 %, respectively.

Ammonium sulfate particles were continuously present in the inflow of the CMFR. The surfaces of these particles served as a suspended substrate to accommodate the gas-to-particle condensation of the oxidation products of β-caryophyllene. An ammonium sulfate solution (Sigma-Aldrich, ≥ 99.0 %) was atomized (TSI, 3076, Liu and Lee, 1975) to produce a polydisperse particle population, which was then dried in a 160-cm silica gel diffusion dryer (RH < 10 %). A monodisperse electric-mobility fraction was selected from the population by a differential mobility analyzer (TSI, 3071 DMA; ^{85}Kr bipolar charger) (Knutson and Whitby, 1975). The DMA was operated with 10 l min^{-1} sheath and 2 l min^{-1} aerosol flows. Electric-equivalent (+1 charge) mobility diameters $d_{m,+1}$ of the seed particles for each experiment are summarized in Table 2. The corresponding surface area concentration inside the CMFR prior to initiating β-caryophyllene ozonolysis was $(4.0 \pm 2.0) \times 10^{-5}\,m^2\,m^{-3}$. For experiments at the highest initial β-caryophyllene concentration of 46.4 ppbv, polydis-

Table 1. Compilation of experimental conditions and particle mass yields reported in the literature for β-caryophyllene oxidation.

Reference	[VOC][a] (ppbv)	[O_3] (ppbv)	T (K)	RH (%)	Scavenger for OH or CI[b]	[NO_x] (ppbv)	Seed	ρ_{org} (kg m^{-3})[c]	ΔM_{org} (µg m^{-3})	Y (%)
Dark ozonolysis at low NO_x										
Grosjean et al. (1993)	540	80	–	–	Cyclohexane	< 1	None	–	–	12
Jaoui et al. (2003)	601	640	287–290	80–85	None	< MDL[d]	None	–	–	62[e]
Lee et al. (2006a)	88	> 350	293	6	Cyclohexane	< 5	AS[f]	1250	336	45
Winterhalter et al. (2009)	305–331	200	296	Dry	HCOOH	–	None	1000	310–660	19–41
	239–315	100–200	296	Dry	HCHO	–	None	1000	130–180	9–12
	258–566	100–200	296	Dry	None	–	None	1000	50–370	6–24
	295–296	200	296	36	None	–	None	1000	420–440	27–28
This study[g]	1–46	50–200[h]	298	40	Cyclohexane	< 1	AS	1200–1600	0.5–230	8–70
Photooxidation										
Hoffmann et al. (1997)	100–102	–	316–322	–	None	268–283	AS	1000	845–998	103–125
Griffin et al. (1999)	6–13	–	307–309	–	None	24–54	AS	1000	18–82[i]	37–79
Lee et al. (2006b)	37	–	295	56	None	25–40	None	1250	212	68

[a] The reacted VOC concentration depends on ozone or OH concentration. [b] Criegee intermediate. [c] The SOM densities are measured values in this study and assumed values in other studies. [d] Minimum detection limit of the NO_x analyzer (Thermo 8440E). [e] Calculated from the reported carbon yield of 39 % by applying an OM : OC ratio of 1.6. [f] Dry ammonium sulfate particles. [g] Other results are reported in Li et al. (2011) and Chen et al. (2011). [h] Steady-state concentrations (i.e., excess ozone concentrations). [i] Particle measurements were conducted outside the reactor at 298 K.

perse seed particles were used instead of monodisperse ones so that the surface area concentration (2.0×10^{-3} m^2 m^{-3}) was sufficiently high to prevent new particle formation by homogeneous nucleation of the organic gases.

In a series of experiments, the initial concentration of β-caryophyllene inside the CMFR prior to ozonolysis was varied from 0.8 to 46.4 ppbv. A liquid solution (1:2500, v/v) of β-caryophyllene (Sigma-Aldrich, $\geq$ 98.5 %) in cyclohexane (Sigma-Aldrich, $\geq$ 99.9 %) was fed by a syringe pump into a round-bottom flask warmed to 70 °C. A continuous flow of air swept the evaporated molecules of β-caryophyllene and cyclohexane from the flask into the CMFR for the entire experimental period. The concentration of β-caryophyllene inside the CMFR was adjusted by using a variable rate of liquid injection from the syringe pump. Cyclohexane served as a scavenger of hydroxyl radicals produced by some ozonolysis pathways. A quadrupole proton-transfer-reaction mass spectrometer (Ionicon, PTR-MS) was used both to confirm the β-caryophyllene concentration in the CMFR prior to ozone injection and to track the extent of reaction after ozone injection (Shilling et al., 2008). Ozone concentrations of 50, 100, and 200 ppbv were used during the conducted experiments (Table 2). Within a single experiment, the ozone concentration was held constant by feedback control, meaning that sufficient ozone was added to react away nearly all the β-caryophyllene while maintaining a constant concentration of 50, 100, or 200 ppbv. For all experiments, the ozone concentrations were therefore in excess compared to the reacted concentrations of β-caryophyllene.

The outflow of the CMFR was continuously sampled by a scanning mobility particle sizer (TSI, 3936L22 SMPS, Wang and Flagan, 1989), by filter-based collection for offline molecular analysis using an ultra-performance liquid chromatography coupled to an electrospray-ionization time-of-flight mass spectrometer (Waters, ACQUITY/LCT Premier XE UPLC-ESI-ToF-MS, Neue et al., 2010), and by an on-line particle-vaporization electron-impact high-resolution time-of-flight mass spectrometer (Aerodyne, HR-ToF-AMS, DeCarlo et al., 2006). The SMPS provided measurements of the number-diameter distribution of the particle population. The UPLC-ESI-ToF-MS molecular analysis of the material sampled onto the filters was previously presented in Li et al. (2011). The HR-ToF-AMS was used for the in situ collection of the mass spectrum of the particle population in the CMFR outflow. During a single steady-state experiment, no significant changes in the mass spectra were observed, and the AMS data sets under steady-state conditions were averaged for 4 to 12 h to increase the signal-to-noise ratio. The measured quantities at steady state typically fluctuated within 5 % during the course of an experiment. The particle population largely had diameters within the AMS acceptance window of 50 to 1000 nm vacuum aerodynamic diameter. The error in M_{org} because of undetected particles is estimated as smaller than 1 % based on the SMPS number-diameter measurements. For experiment #27 (Table 2), a DMA (TSI, 3071; ^{85}Kr bipolar charger) was coupled to an aerosol particle mass analyzer (Kanomax, APM 3600, Ehara et al., 1996) to measure the particle effective density.

The CMFR was an experimental configuration that facilitated the study of ultimate yield by providing a mean residence time sufficient for multi-generational chemistry (Kleindienst et al., 1999). For example, the lifetime of β-caryophyllene was 20 s based on a rate constant of $(1.2 \pm 0.1) \times 10^{-14}$ molecule^{-1} cm^3 s^{-1} at 200 ppbv ozone.

Table 2. Experimental conditions and results for the dark ozonolysis of β-caryophyllene. The terms ΔVOC, $(M_{org})_{outflow}$, $M_{org,corr}$, and $\overline{OS}_c$, respectively represent the reacted concentration of the precursor VOC in an experiment, the mass concentration of particle-phase SOM measured by the AMS, the mass concentration of particle-phase SOM corrected by wall loss and used in the yield calculation (Eq. 2), and the average oxidation state of carbon for particle-phase SOM, calculated as 2(O : C) – 1(H : C) (Kroll et al., 2011). The O : C and H : C ratios were originally reported in Chen et al. (2011). Material density ρ_{org} is reported only for experiments using monodisperse seed and having $(M_{org})_{outflow} > 1\,\mu g\,m^{-3}$. Errors represent the measurement precision. For Exp. #10, a ^{210}Po charger was installed in the seed injection line, which neutralized the charged particles exiting the DMA and prior to entering the chamber. As a result of neutralization, electrostatic particle loss to the bag walls decreased (McMurry and Rader, 1985).

Exp. No	Date	Reaction conditions			Measured quantities			Derived quantities at steady state					
		Seed diameter $d_{m,+1}$ (nm)	ΔVOC (ppbv)	$[O_3]_{ss}$ (ppbv)	$(M_{org})_{outflow}$ ($\mu g\,m^{-3}$)	O : C	H : C	ρ_{org} (AMS-SMPS) ($kg\,m^{-3}$)	OM : OC	$\overline{OS}_c$	β (h^{-1})	$M_{org,corr}$ ($\mu g\,m^{-3}$)	Y (%)
1	3 Apr 2009	68.5	1.6	50	0.4 ± 0.0	0.49	1.51	–	1.82	–0.54	1.04 ± 0.11	1.8 ± 0.2	13.2 ± 1.2 %
2	12 Apr 2009	68.5	3.1	50	1.1 ± 0.0	0.49	1.49	1810 ± 190	1.79	–0.51	1.04 ± 0.11	5.3 ± 0.4	20.4 ± 1.7 %
3	17 Apr 2009	68.5	6.3	50	3.4 ± 0.1	0.45	1.48	1450 ± 110	1.73	–0.58	1.04 ± 0.11	15.8 ± 1.4	30.1 ± 2.7 %
4	18 Apr 2009	68.5	6.4	100	4.3 ± 0.3	0.45	1.49	1400 ± 130	1.73	–0.59	1.04 ± 0.11	20.0 ± 2.0	37.4 ± 3.8 %
5	20 Apr 2009	68.5	6.5	200	6.3 ± 0.2	0.43	1.49	1520 ± 90	1.71	–0.62	1.04 ± 0.11	29.6 ± 2.6	54.8 ± 4.9 %
6	23 Apr 2009	68.5	12.9	50	9.3 ± 0.4	0.40	1.48	1330 ± 60	1.66	–0.69	1.04 ± 0.11	44.4 ± 4.1	41.3 ± 3.8 %
7	26 Apr 2009	68.5	13.2	200	15.9 ± 0.3	0.36	1.49	1300 ± 70	1.61	–0.77	1.04 ± 0.11	75.8 ± 6.5	68.7 ± 5.9 %
8	6 May 2009	49.5	0.8	50	0.1 ± 0.0	0.53	1.57	–	1.90	–0.51	1.04 ± 0.11	0.5 ± 0.1	8.0 ± 1.0 %
9	7 May 2009	49.5	1.6	50	0.4 ± 0.0	0.53	1.52	–	1.87	–0.46	1.04 ± 0.11	1.7 ± 0.2	13.0 ± 1.2 %
10	8 May 2009	49.5	1.6	100	0.9 ± 0.0	0.51	1.49	–	1.83	–0.47	0.49 ± 0.03	2.5 ± 0.1	18.6 ± 0.9 %
11	9 May 2009	49.5	1.6	200	0.4 ± 0.0	0.53	1.51	–	1.86	–0.45	1.04 ± 0.11	1.9 ± 0.2	14.6 ± 1.7 %
12	12 May 2009	49.5	3.2	50	0.8 ± 0.0	0.53	1.51	–	1.85	–0.46	1.04 ± 0.11	3.7 ± 0.3	13.6 ± 1.2 %
13	14 May 2009	49.5	3.3	100	0.9 ± 0.0	0.53	1.50	–	1.85	–0.43	1.04 ± 0.11	4.5 ± 0.4	16.3 ± 1.4 %
14	15 May 2009	49.5	3.3	200	1.3 ± 0.0	0.53	1.50	1520 ± 100	1.85	–0.44	1.04 ± 0.11	6.1 ± 0.5	21.9 ± 2.0 %
15	17 May 2009	49.5	6.4	50	3.2 ± 0.0	0.50	1.48	1430 ± 140	1.80	–0.48	1.04 ± 0.11	15.2 ± 1.3	28.4 ± 2.4 %
16	19 May 2009	49.5	6.5	100	4.2 ± 0.1	0.49	1.49	1400 ± 110	1.79	–0.50	1.04 ± 0.11	19.9 ± 1.7	36.6 ± 3.1 %
17	20 May 2009	49.5	6.6	200	5.3 ± 0.2	0.48	1.49	1370 ± 100	1.77	–0.53	1.04 ± 0.11	25.3 ± 2.3	46.1 ± 4.2 %
18	23 May 2009	49.5	12.8	50	9.3 ± 0.2	0.42	1.48	1360 ± 70	1.69	–0.65	1.04 ± 0.11	44.4 ± 3.8	41.4 ± 3.6 %
19	26 May 2009	49.5	13.1	100	10.8 ± 0.1	0.39	1.48	1330 ± 60	1.65	–0.69	1.04 ± 0.11	51.4 ± 4.3	47.2 ± 4.0 %
20	29 May 2009	49.5	13.4	200	16.1 ± 0.4	0.37	1.48	1340 ± 80	1.62	–0.75	1.04 ± 0.11	77.4 ± 6.8	69.5 ± 6.1 %
21	4 Jun 2009	49.5	1.6	50	0.4 ± 0.0	0.53	1.52	–	1.85	–0.46	1.04 ± 0.11	1.8 ± 0.2	13.4 ± 1.2 %
22	5 Jun 2009	49.5	1.7	200	0.6 ± 0.0	0.53	1.51	–	1.85	–0.45	1.04 ± 0.11	2.8 ± 0.3	20.3 ± 1.8 %
23	7 Jun 2009	49.5	1.6	100	0.5 ± 0.0	0.54	1.51	–	1.89	–0.39	1.04 ± 0.11	2.1 ± 0.2	15.8 ± 1.4 %
24	12 Jun 2009	poly	45.7	100	47.7 ± 0.5	0.33	1.48	–	1.56	–0.82	1.04 ± 0.11	227.1 ± 19.2	59.6 ± 5.0 %
25	17 Jun 2009	49.5	13.0	100	8.4 ± 0.2	0.41	1.48	1260 ± 50	1.68	–0.66	1.04 ± 0.11	40.0 ± 3.5	36.8 ± 3.2 %
26	18 Jun 2009	poly	44.9	50	36.3 ± 1.7	0.33	1.47	–	1.57	–0.81	1.04 ± 0.11	172.6 ± 16.6	46.0 ± 4.4 %
27	14 Sep 2010	46.1	13.0	50	18.2 ± 0.2	0.35	1.47	1230 ± 60	1.57	–0.77	0.19 ± 0.02	30.7 ± 1.3	28.7 ± 1.3 %

The average ozonolysis lifetime of the first-generation products of β-caryophyllene was about 0.5 h (1860 s) based on a rate constant of $(1.1 \pm 0.4) \times 10^{-16}$ molecule^{-1} cm^3 s^{-1} (Shu and Atkinson, 1995; Winterhalter et al., 2009). In comparison, the mean residence time of the Harvard Environmental Chamber for most experiments was 3.6 h (13 100 s) (Shilling et al., 2008; King et al., 2009). The CMFR operation also improved the precision and accuracy of yield measurements at low M_{org} by providing sufficient observation time for significant signal averaging (Shilling et al., 2008). By establishing a steady state and thereby saturating the surface layers of the Teflon bag material (Matsunaga and Ziemann, 2010), CMFR operation also reduced the effects of wall interactions on reactive and non-reactive exchanges with gas-phase molecules, including the re-partitioning of condensable products (cf. further discussion in the Sect. A of the Supplement).

2.2 AMS data analysis

The spectra collected by the HR-ToF-AMS were used to calculate the mass concentrations and the elemental ratios of the particle-phase secondary organic material present in the outflow from the CMFR (Table 2). The spectra were analyzed using the software toolkits Sequential Igor Data Retrieval (SQUIRREL), Peak Integration by Key Analysis (PIKA), and Analytic Procedure for Elemental Separation (APES) (DeCarlo et al., 2006; Aiken et al., 2007). In the analysis, standard relative ionization efficiencies (RIE) were used, corresponding to 1.1 for nitrate, 1.2 for sulfate, 1.4 for organic molecules, 4.0 for ammonium, 1.3 for chloride, and 2.0 for water (Alfarra et al., 2004; Mensah et al., 2011). An AMS collection efficiency (a factor which potentially corrects for undetected particle mass concentration) of 1.0 was used, as supported by the agreement of the AMS-measured mass concentrations with the density-compensated volume concentrations measured by the SMPS (Sect. 2.3). Determination of the air correction factors, several updates to the fragmentation table, and the contributions of organic material to CO^+ and H_xO^+ signal intensities followed the method described in Chen et al. (2011).

2.3 Material density

Under an assumption of spherical particles, volume-diameter distributions measured by the SMPS can be used in conjunction with mass-diameter distributions measured by the AMS to estimate the particle effective density ρ_{eff} (kg m^{-3}). More specifically, ρ_{eff} was calculated by dividing the mass-mode particle diameter measured by the AMS (i.e., vacuum aerodynamic diameter) by the volume-mode diameter measured by the SMPS (i.e., mobility diameter) (DeCarlo et al., 2004; Bahreini et al., 2005; Katrib et al., 2005). Figure S1 shows two examples of the mass-diameter distribution derived from the SMPS measurements compared to that measured by the AMS for particles in the CMFR outflow. The SMPS mass-diameter distributions were derived by multiplying the SMPS volume-diameter distributions by the ρ_{eff} value that was obtained using the mode diameters. The good agreement between the SMPS and AMS distributions suggests that within detection limits ρ_{eff} does not vary with diameter. The integrated area under the distributions represents the total particle mass concentration. Figure S2 shows the scatter plot of the total mass concentrations obtained from the AMS measurements against the SMPS-derived concentrations. The slope of 0.99 ± 0.02 indicates that an AMS collection efficiency of unity can be assumed given the measurement uncertainties of the AMS and the SMPS (Matthew et al., 2008; Shilling et al., 2008).

For nonporous spherical particles, effective density is identical to material density (DeCarlo et al., 2004). Past work indicates the applicability of a nonporous spherical morphology for SOM-coated sulfate particles (King et al., 2007). Based on the ρ_{eff} value obtained for each experiment, the material density ρ_{org} of the SOM was calculated by the rule of volume additivity. As explained by Bahreini et al. (2005), in context of AMS data sets this rule states that $\rho_{org} = M_{org} / \left(M_{particle} / \rho_{eff} - M_{AS} / \rho_{AS} \right)$, where ρ_{AS} is the material density of ammonium sulfate (1770 kg m^{-3}), $M_{particle}$ is the total particle mass concentration (µg m^{-3}), and M_{AS} is the ammonium sulfate mass concentration (µg m^{-3}). The presented equation is valid provided that the chemical components either do not mix or alternatively have a numerically small excess volume of mixing. The ρ_{org} values obtained by this analysis and their uncertainties are listed in Table 2. The uncertainties of 5 to 10 % were based on a Monte Carlo analysis. The parameters used in the analysis included the uncertainty in the SMPS and AMS mode diameters (i.e., as needed for calculating ρ_{eff}) as well as the standard deviations of the temporal variation of $M_{particle}$, M_{org}, and M_{AS} at steady state.

For experiment #27 (Table 2), independent measurements of ρ_{eff} and hence independent calculations of ρ_{org} were also made by the DMA-APM methodology (Kuwata et al., 2012). In this case, ρ_{org} was calculated from data of quasi-monodisperse particles rather than for the entire particle population. The uncertainty of ρ_{org} for the DMA-APM method was estimated as 2 % on the basis of calibrations using polystyrene latex particles.

Figure S3 shows that the ρ_{org} values determined by the independent AMS-SMPS and DMA-APM methods were in agreement. The measured value of ρ_{org} of 1320 ± 20 kg m^{-3} at high mass concentrations ($M_{org} > 50$ µg m^{-3}) was also consistent with the value reported previously by Bahreini et al. (2005) for β-caryophyllene ozonolysis for experiments at $M_{org} = 300$ µg m^{-3}. Figure S3 also shows that there was a dependence of ρ_{org} on organic particle mass concentration. A similar result was reported previously for α-pinene ozonolysis (Shilling et al., 2009).

2.4 Particle mass yield

Particle mass yield Y is defined as $Y \equiv \Delta M_{org}/\Delta VOC$, with the sign construed as positive. The term ΔVOC is the difference in the β-caryophyllene concentration between the outflow and the inflow of the CMFR, meaning that negligible loss to any apparatus surface is assumed for unreacted β-caryophyllene at steady state. The accuracy of this assumption was supported by the agreement between the β-caryophyllene concentrations in the CMFR outflow prior to initiation of reaction (as measured by the PTR-MS) and the concentrations calculated using the liquid injection rate of the syringe pump.

For ΔM_{org}, a simplification is that the inflow concentration is zero but a complication is that significant mass is lost to the walls of the bag and therefore does not contribute to concentration measured in the outflow. Therefore, $\Delta M_{org} = (M_{org})_{outflow} + (M_{org})_{wallloss} - (M_{org})_{inflow}$. We measure $(M_{org})_{outflow}$ using the AMS, we know $(M_{org})_{inflow} = 0$, and we relate $(M_{org})_{wallloss} = f((M_{org})_{outflow})$ by calibration of wall-loss rates. More specifically, $(M_{org})_{wallloss} = \beta\ \tau\ (M_{org})_{outflow}$ for an assumed first-order diameter-independent particle wall-loss coefficient β (s^{-1}) and a mean residence time τ (s) in the CMFR (Seinfeld et al., 2003; Pierce et al., 2008). Wall-loss mechanisms include Brownian diffusion, electrostatic forces, and gravitational sedimentation (McMurry and Grosjean, 1985). The final form of the equation for particle mass yield for the conducted experiments is as follows:

$$Y = \left| \frac{(1+\beta\tau)(M_{org})_{outflow}}{VOC_{outflow} - VOC_{inflow}} \right| \quad (1)$$

For further use, we also introduce here the definition $M_{org,corr} \equiv (1+\beta\ \tau)(M_{org})_{outflow}$ as the wall-loss corrected organic particle mass concentration. Derivation of this equation is provided in the Sect. A of the Supplement.

The particle wall-loss coefficient β can be determined experimentally by measuring the change in number concentration of surrogate particles in the chamber (McMurry and Grosjean, 1985). For this purpose, experiments were conducted with populations of ammonium sulfate particles in the absence of organic material. On the basis of the particle number balance in the CMFR (Seinfeld et al., 2003), $\beta = (2.9 \pm 0.3) \times 10^{-4}\ s^{-1}$ was obtained, and no significant dependence of β on diameter was observed for the studied populations (Fig. 1). For number-diameter distributions of SOM-coated sulfate particles of the actual experiments (Fig. S4), independent estimates of $\beta = (2.8 \pm 0.4) \times 10^{-4}\ s^{-1}$ were obtained by comparing the total particle number concentrations measured in the CMFR outflow to the total concentrations expected based on the seed particle concentrations in the CMFR inflow.

The measured wall-loss coefficients of the present study were greater than the measured values for the earlier experiments in the Harvard Environmental Chamber.

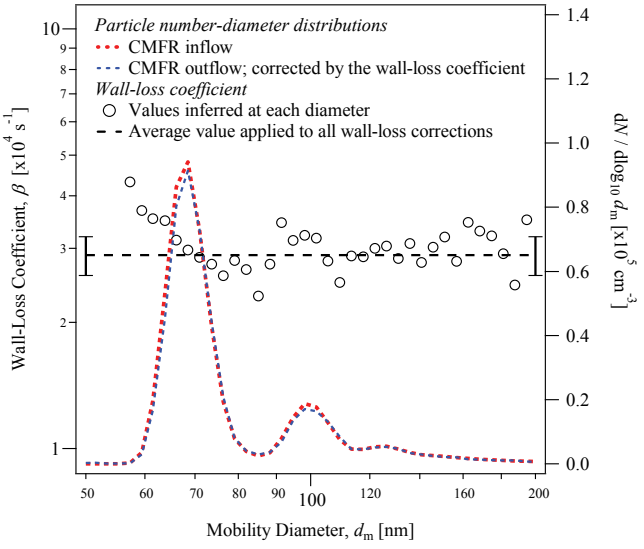

Fig. 1. Measurement of particle wall-loss coefficients β (s^{-1}) in the Harvard Environmental Chamber. Data are shown for one experiment using a population of dry ammonium sulfate particles. Points show the wall-loss coefficient inferred at each diameter such that the outflow number-diameter distribution matches the inflow distribution. No trend with particle diameter is apparent. Therefore, wall losses are accurately represented by an average value, shown by the dotted line, for the investigated particle population. The error bars represent one-sigma standard deviation of three replicate experiments.

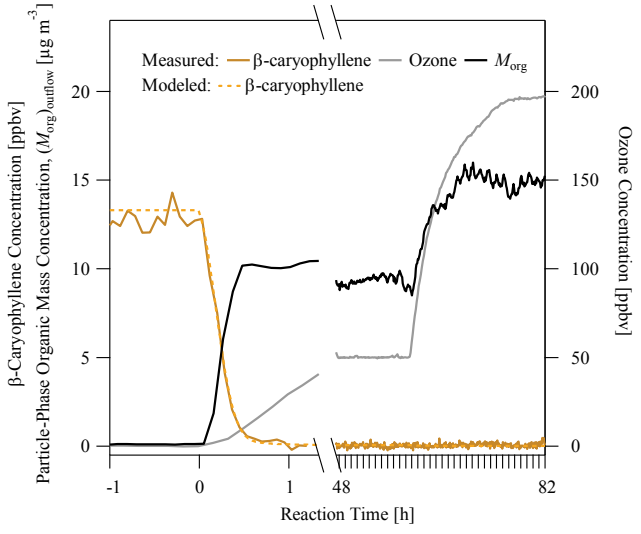

Fig. 2. A typical time series for the transient phase of the CMFR showing the loss of β-caryophyllene, the appearance of particle-phase secondary organic material following the introduction of ozone, and the increase of particle-phase organic material following the elevation of ozone concentration.

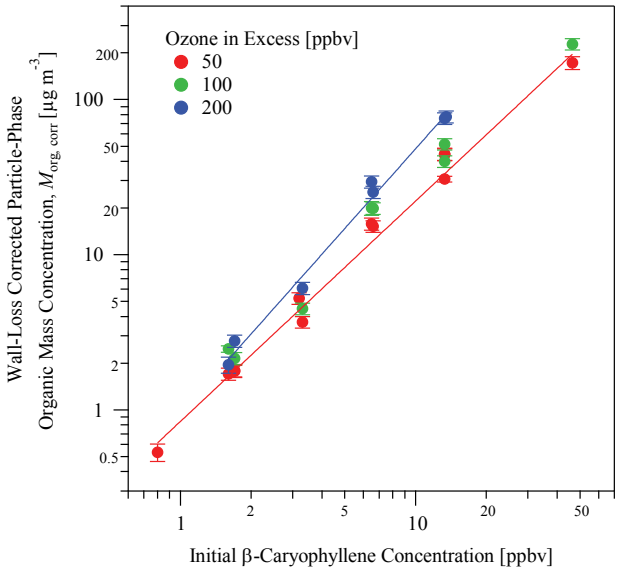

Fig. 3. Organic particle mass concentrations at steady state in the CMFR for increasing initial concentration of β-caryophyllene and three different ozone concentrations. The plotted concentrations are corrected for wall loss (Eq. 1). Uncertainties shown for the data points represent the propagated standard deviation (one sigma) of both the temporal variation of M_{org} as well as the wall-loss corrections. Lines are shown to guide the eye.

Shilling et al. (2008) reported $\beta = 4.7$ to $2.5 \times 10^{-5}\,s^{-1}$ for dry ammonium sulfate particles of 50 to 150 nm. The explanation for the difference is the use of an aged bag in the study of Shilling et al. (2008) and a new Teflon bag for most experiments of the present study. In support of this explanation, the experiments described herein from April to June 2009 correspond to the reported β values, and no systematic temporal trend of wall losses was observed during this time period, suggesting that the effects of bag aging during the two months of experiments were minimal. In September 2010, with the by-then aged bag, β values in agreement with Shilling et al. (2008) were obtained, as represented by experiment #27 of Table 2. The additional aging of the bag surface significantly decreased the particle wall losses, perhaps because of surface alterations that influenced electrostatic charging (McMurry and Rader, 1985). In support of this explanation, re-neutralization of the seed particles prior to the injection decreased particle wall losses, as represented by experiment #10 of Table 2.

Experiments carried out at repeated conditions show differences no more than 30 %, supporting the reproducibility of the results (Table 2). The particle-phase organic mass concentrations were corrected by 68 to 370 % for the different β values of the experiments (Eq. 1). The corrected values lay on a self-consistent trend line within instrument uncertainty, supporting the accuracy of the applied corrections (Fig. S5).

3 Results and discussion

Figure 2 shows a typical time series for the transient period prior to steady-state in the CMFR. The time traces show the loss of β-caryophyllene after the introduction of ozone and the appearance of particle-phase secondary organic material. Seed particles and β-caryophyllene were introduced into the CMFR and reached steady-state concentrations prior to the injection of ozone. Once ozone was introduced, the concentration of β-caryophyllene decreased rapidly. After a transient period, feedback control between the measured ozone concentration and the quantity of ozone injected into the bag maintained the ozone concentration at 50 ppbv. The steady-state concentrations of particle-phase SOM were reached after 8 h and were maintained until completion of the experiment after 56 h.

During the transient period of Fig. 2, the initial consumption of β-caryophyllene was primarily by the reaction of ozone with the endo-cyclic double bond. The ozonolysis rate constant of the endo-cyclic double bond of β-caryophyllene ($k_{endo} = 1.16 \times 10^{-14}$ molecule^{-1} cm^3 s^{-1}) is 100× greater than that of the exo-cyclic double bond of the first-generation products ($k_{exo} = 1.1 \times 10^{-16}$ molecule^{-1} cm^3 s^{-1}) (Shu and Atkinson, 1995; Winterhalter et al., 2009). The time decay of the β-caryophyllene concentration agreed well with that predicted for the CMFR (i.e., the modeled line in Fig. 2) using the rate constant k_{endo} and the measured ozone concentrations.

Subsequent to the first transient period, Fig. 2 shows that a further increase in the ozone concentration to 200 ppbv caused an increase in the mass concentration of particle-phase SOM. The remaining exo-cyclic double bond of the first-generation products reacted at the higher ozone concentration, leading to additional low-volatility products that partitioned to the particle phase (Kanawati et al., 2008; Li et al., 2011). The data of Fig. 3 demonstrate the generalization of this result for a single injected β-caryophyllene concentration to all experiments, showing an increase in yield for 200 compared to 50 ppbv ozone for all injected β-caryophyllene concentrations.

The representation in Fig. 2 can be put into a quantitative context by comparing the ozone-dependent e-folding lifetimes $\tau_{endo}(O_3)$ and $\tau_{exo}(O_3)$ of the two double bonds at 50 and 200 ppbv (i.e., $\tau(O_3) = 1/k[O_3]$) to the mean CMFR residence time τ_{CMFR}. The values are as follows: $\tau_{endo}(50) = 70$ s, τ_{endo} $(200) = 20$ s, $\tau_{exo}(50) = 7500$ s, $\tau_{exo}(200) = 2000$ s, and $\tau_{CMFR} = 13\,100$ s. The relationships $\tau_{CMFR}/\tau_{endo}(50) \gg 10$ and $\tau_{CMFR}/\tau_{endo}(200) \gg 10$ imply that β-caryophyllene is consumed to nearly 100 % for both ozone concentrations. This result is supported by the PTR-MS measurements that show a negligible residual β-caryophyllene concentration in the CMFR outflow for 50 and 200 ppbv ozone (Fig. 2).

The population of first-generation products i has a distribution of reactivity $\tau_{exo,i}$ with respect to ozonolysis

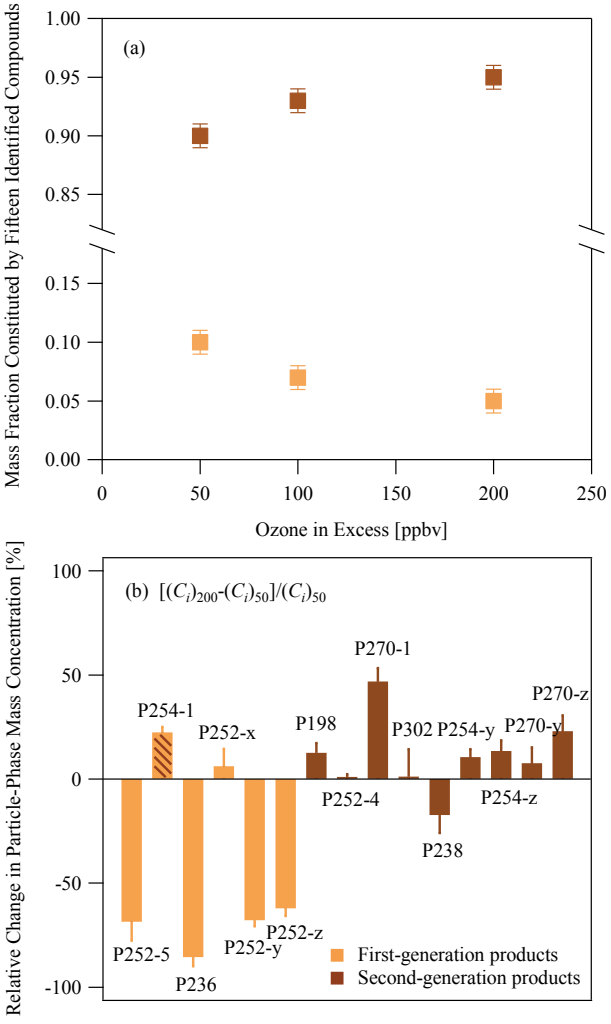

Fig. 4. **(a)** Mass fractions of first- and second-generation products for increasing ozone concentration, as quantified by UPLC-ESI-ToF-MS. The ordinate of mass fraction represents the sum of the mass concentrations of either the first- or second-generation products divided by the combined sum of first- and second-generation mass concentrations, all measured by UPLC-ESI-ToF-MS for filter-extracted samples (Li et al., 2011). **(b)** The percent change in mass concentration at 50 compared to 200 ppbv O_3 for the fifteen identified products. Experiments in this figure are for 13 ppbv of reacted β-caryophyllene. Error bars represent the one-sigma standard deviation of three replicate experiments. Labels x, y, and z represent a permutation of 1, 2, and 3. P254-1 is hashed because the data of the present study suggest that this product might have been assigned incorrectly in previous work as a first-generation product (Li et al., 2011); it can instead be assigned as a second-generation product (see main text).

of the remaining exo-cyclic double bond. This distribution in reactivity is assumed to be represented by a mean value τ_{exo} and an associated variance σ^2 for the population of products. The calculations $\tau_{CMFR}/\tau_{exo}(50) = 1.8$ and $\tau_{CMFR}/\tau_{exo}\ (200) = 6.6$ suggest that for many products i the relationships $0.1 < \tau_{CMFR}/\tau_{exo,i}(50) < 10$ and $0.1 < \tau_{CMFR}/\tau_{exo,i}\ (200) < 10$ hold, implying that there are significant differences among the various first-generation products in the timescales for conversion from first- to second-generation products. These differences are sensitive to the ozone concentration in the CMFR. For instance, a kinetics calculation (cf. Sect. B of the Supplement) suggests a mean conversion of 63 % from first- to second-generation products for 50 ppbv ozone compared to a mean conversion of 87 % for 200 ppbv ozone. The actual overall conversion to second-generation products depends upon the unknown probability density function PDF(τ_{exo},σ) of reactant concentrations and reactivity. The experimental observations of Fig. 2 show that there is a 60 % increase in $(M_{org})_{outflow}$ for 200 compared to 50 ppbv ozone. This increase is caused by the additional conversion of first- to second-generation products at 200 ppbv ozone.

Differences in particle-phase molecular products between 50 and 200 ppbv ozone exposure, as highlighted in Fig. 4, are consistent with an enhancement of second-generation products relative to first-generation ones. Figure 4a shows the ozone-dependent mass fractions of first- compared to second-generation products, as determined by UPLC-ESI-ToF-MS for 15 compounds (Li et al., 2011). As the ozone concentration increases, the second-generation products are increasingly dominant.

Figure 4b shows the percent change in mass concentration for exposure to 50 compared to 200 ppbv ozone for each of the 15 products. The structures of the products labeled in Fig. 4 are provided in Li et al. (2011) and are reproduced for convenience in Fig. S6. Figure 4b shows that the mass concentrations of the first-generation products decrease and the concentrations of the second-generation products increase at higher ozone concentration, as is consistent with the conversion of the former into the latter. The concentration of P270-1 represents the largest relative change, possibly suggesting that its first-generation precursor compound has a relatively low ozonolysis rate constant. There are, however, a few exceptions apparent to this trend. Unlike other second-generation products, the mass concentrations of the products P252-4 and P302 do not change, suggesting that at 50 ppbv ozone they are already produced to completion from their first-generation precursors. Another exception is P238, showing a negative relative change in mass concentration. This species is produced from the first-generation product P236 by a stabilized Criegee intermediate channel that competes with an RO_2-assisted isomerization channel (Fig. S6). At higher ozone concentrations, the importance of the isomerization channel possibly increases because of higher RO_2 concentrations, providing one possible explanation for the observed decrease in P238 concentration.

Unlike other first-generation products, the mass concentrations of the products P252-x and P254-1 increase at 200 ppbv ozone. The relative concentration change of P252-x is

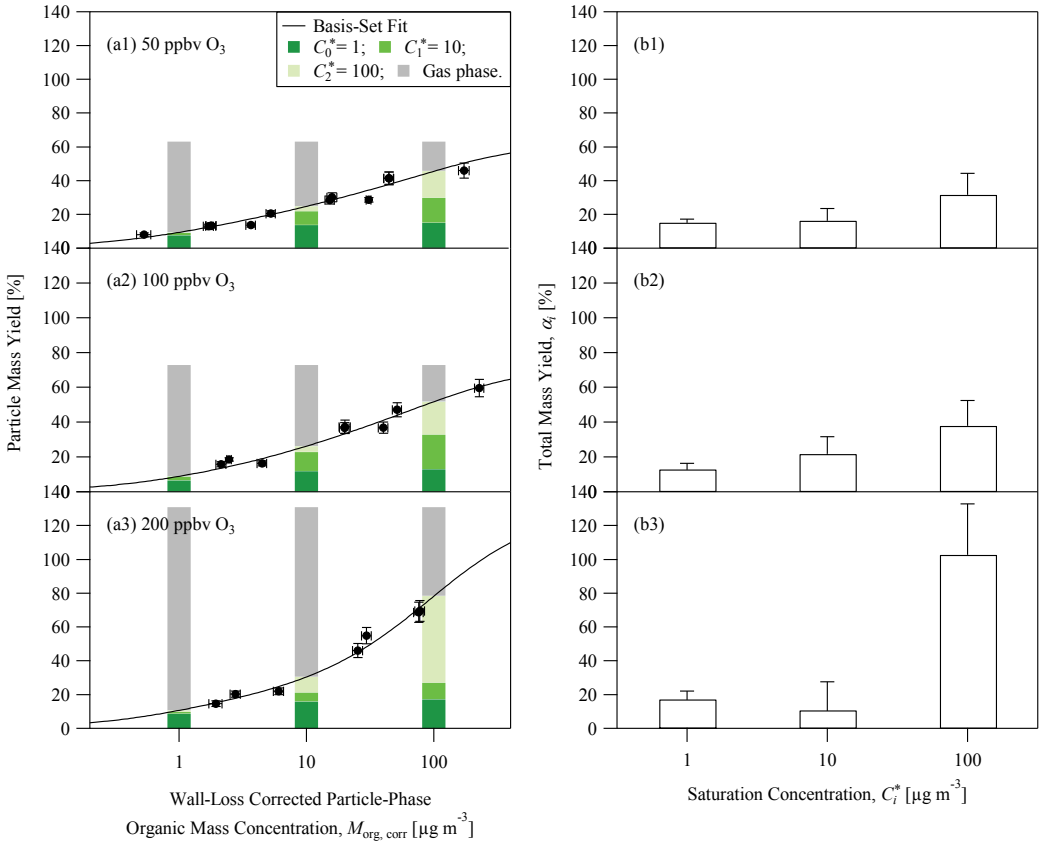

Fig. 5. (a1–a3) Particle mass yield and basis-set parameterization for the dark ozonolysis of β-caryophyllene. (b1–b3) Optimized parameter α_i for product classes of C_i^*= {1, 10, 100} µg m^{-3}. Data are shown for 50, 100, and 200 ppbv ozone.

negligible given the uncertainty. In this case, we can assign x = 1 because the second-generation product of P252-1 (i.e., P302) also changes negligibly but the products of P252-2 and P252-3 (i.e., P270-y, P270-z, P254-y, and P254-z) all show positive changes (Fig. S6). P254-1 was assigned previously as the first-generation product β-caryophyllinic acid, which has been observed in ambient samples and used as a tracer for β-caryophyllene SOM (Jaoui et al., 2007; Kleindienst et al., 2007; Hu et al., 2008). A second-generation product (β-nocaryophyllonic acid), however, has the same exact mass at P254-1 (Jaoui et al., 2003; Chan et al., 2011). The increased mass concentration of P254-1 for 200 ppbv ozone (Fig. 4b) suggests that P254-1 might be incorrectly assigned in Li et al. (2011) as β-caryophyllinic acid and that P254-1 should instead be assigned as the second-generation product β-nocaryophyllonic acid.

Figure 5 presents the yield data for increasing organic particle mass concentration. Yield data are customarily parameterized with the objective of further upscale modeling (e.g., air quality models). In common usage, parameterizations are based on either a two-product mode (Odum et al., 1996) or a basis-set approach (Presto and Donahue, 2006). Our application employs the latter. The products formed by the oxidation of β-caryophyllene are binned into product classes of mass yields α_i, and the volatilities of the product classes are prescribed in decadal units of 10^{-i}, where 10^{-i} is denoted as C_i^*. Particle mass yield is then written (Seinfeld and Pankow, 2003; Presto and Donahue, 2006):

$$Y(M_{\text{org,corr}}) \equiv \frac{\Delta M_{\text{org}}}{\Delta \text{VOC}} = \sum_{i=i_i}^{i_f} \alpha_i \left(1 + \frac{C_i^*}{M_{\text{org,corr}}}\right)^{-1} \quad (2)$$

The yield data sets in panels a1–a3, which represent the three different ozone concentrations of this study, were each fit using Eq. (1) for $i_i = 0$ and $i_f = 2$. The fit treated C_i^*(µg m^{-3}) as fixed quantities, Y and $M_{\text{org,corr}}$ as data, and α_i as the quantities for optimization. The overall bar height in panels a1–a3 represents the cumulative potential yield (i.e., $\sum_{i=i_i}^{i_f} \alpha_i$). The coloring inside each bar represents the partitioning of the organic molecules between the gas (gray) and particle (green) phases (Donahue et al., 2006; Presto and Donahue, 2006). The different shades of green represent the volatility associated with a component of the particle phase. The optimized values for α_i (Table S1) are plotted in the panels b1–b3 for each ozone concentration.

An approximate upper limit of 150 % for the maximum potential particle mass yield from β-caryophyllene ozonolysis can be established by assuming that two ozone molecules add to the original molecule and that all product molecules partition to the particle phase. The representation in panel a1 of Fig. 5 shows that the cumulative yield approaches 60 % for 50 ppbv ozone. By comparison, panel a3 for 200 ppbv ozone shows that the cumulative yield approaches 130 %, suggesting that the overall reaction is nearly complete. The implication is that the particle-phase mass yield represented by each green bar in panel a3 can be taken as the approximate representation of the ultimate yield.

From 50 to 200 ppbv ozone, the optimized mass yields α_i have similar values for products of low volatility ($C_i^* = 1$, 10 $\mu g\,m^{-3}$) but a trend of increasing values for products of relatively high volatility ($C_i^* = 100\,\mu g\,m^{-3}$) (panels b1–b3 of Fig. 5). The similar values of mass yields suggest that the low-volatility products are mainly second-generation products that are formed nearly to completion from their first-generation precursors even at 50 ppbv, indicating fast formation pathways. In this case, the mass yields are not sensitive to the ozone concentration. Product P302 is the lowest volatility product among the 15 identified products and can therefore be supposed as the dominant species to condense to the particle phase at low M_{org} (Li et al., 2011). This conclusion that P302 is fast-forming low-volatility product is supported by the molecular data; there is a negligible change in the mass concentration for an increase in ozone concentration (Fig. 4b). By comparison, the trend of increasing α_i values with increasing ozone concentration for $C_i^* = 100\,\mu g\,m^{-3}$ suggests that the relatively high-volatility products are mainly second-generation products that are formed by relatively slow pathways. The increase of ozone concentration leads to greater conversion of these products from their first-generation precursors. Panels a1–a3 show the consequence of these processes: the increase in particle mass yield from 50 to 200 ppbv ozone is dominantly driven by products of relatively high volatility (cf. large light-green bar in panel a3 for $C_i^* = 100\,\mu g\,m^{-3}$).

The findings for α_i represented in panels b1–b3 provide a formal framework for the observation that differences in particle mass yield for 200 ppbv compared to 50 ppbv ozone are small for $M_{org,corr} < 10\,\mu g\,m^{-3}$ but greater for higher $M_{org,corr}$ (panels a1–a3). For low $M_{org,corr}$, the particle-phase SOM is dominantly composed of products having low volatility. Therefore, the significantly increased production at 200 ppbv ozone of the high-volatility products of $C_i^* = 100$ $\mu g\,m^{-3}$ causes little additional partitioning to the particle phase. By comparison, for $10 \le M_{org,corr} \le 100\,\mu g\,m^{-3}$ products of $C_i^* = 100\,\mu g\,m^{-3}$ increasingly partition to the particle phase, meaning that 10 % of these products partition to the particle phase for $M_{org,corr} = 10$ $\mu g\,m^{-3}$ and 50 % of them to the particle phase for $M_{org,corr} = 100$ $\mu g\,m^{-3}$ (Donahue et al., 2006).

There is a dependency of the O:C elemental ratio, as measured by the AMS, on $M_{org,corr}$, and this dependency may also be explained by the volatility distribution of the products. The O:C ratios ranges from 0.5 to 0.3, corresponding to an average addition of 5 to 8 oxygen atoms to the C_{15} structure of β-caryophyllene. This average is consistent with a dominant presence of second-generation products in the particle phase because the first-generation products typically have 1 to 4 oxygen atoms (Winterhalter et al., 2009; Li et al., 2011). The experimental results for $M_{org,corr} < 10\,\mu g\,m^{-3}$ show that neither an increase in ΔVOC (Fig. 6a) nor an increase in the steady-state O_3 concentration (Fig. 6b) changes the O:C ratio, at least within measurement uncertainty (O:C $\approx$0.5 and $\overline{OS}_c \approx 0.5$; Table 2). This behavior is consistent with the dominant contribution of low-volatility, fast-forming second-generation products to the particle phase. By comparison, for $M_{org,corr} > 10\,\mu g\,m^{-3}$ the O:C ratio steadily decreases for increasing ΔVOC and ozone concentrations. This correspondence between decreased O:C ratio and increased contribution of high-volatility products (i.e., $C_i^* = 100$ $\mu g\,m^{-3}$) conforms to the expected structure-function relationship between a molecule's oxygen content and its vapor pressure, meaning greater oxygen content of a molecule and an associated decreased vapor pressure (Pankow and Asher, 2008).

The yield data of this study are summarized as a function of $M_{org,corr}$ in Fig. 7, including comparisons to data sets of previous studies. Panel a shows the yield data for $M_{org,corr} < 10\,\mu g\,m^{-3}$, corresponding to atmospheric concentrations. Panel b shows the yield data for a greater range of $M_{org,corr}$. For $M_{org,corr}$ <10 $\mu g\,m^{-3}$, prior to the present study no data are known to us for the particle mass yield of β-caryophyllene ozonolysis. For $M_{org,corr} > 10\,\mu g\,m^{-3}$, two studies have previously been carried out for conditions of excess ozone (Jaoui et al., 2003; Lee et al., 2006a) (Table 1). Jaoui et al. (2003) reported a yield of 62 % but did not report M_{org}, preventing a specific comparison to our data set. Lee et al. (2006a) reported a yield of 45 % for $M_{org} = 336$ $\mu g\,m^{-3}$. This yield is lower than the yield of 55–100 % reported in the present study for similar M_{org}. The differences between the two studies might be related to the employed relative humidity, which was 40 % in our study and 6 % in Lee et al. (2006a). Winterhalter et al. (2009) showed that increased particle mass yields can be expected for higher relative humidity. Figure 7b also shows yields reported for β-caryophyllene photooxidation. Differences in the chemical mechanisms of ozonolysis and photooxidation notwithstanding, Lee et al. (2006b) reported yields approximately similar to those of the present study. The photooxidation yields reported by Griffin et al. (1999), however, are greater than those of the present study. In the case of early stage photooxidation compared to ozonolysis, a possible shift to lower volatility might occur in the product population because of additional oxidation by OH, though the extent of such shift can be expected to depend strongly on reaction conditions.

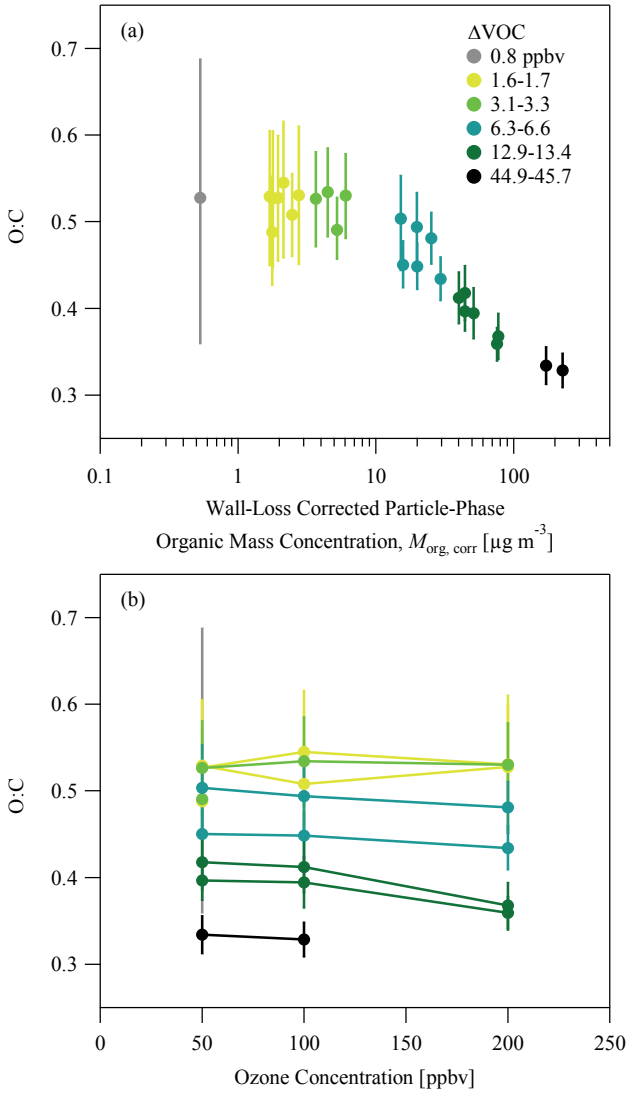

Fig. 6. Oxygen-to-carbon elemental ratios of particle-phase SOM produced by β-caryophyllene ozonolysis for **(a)** increasing particle-phase organic mass concentration and **(b)** increasing ozone concentration. The elemental ratios were determined from the particle-phase high-resolution mass spectra (Aiken et al., 2007, 2008; Chen et al., 2011). Error bars represent the one-sigma measurement precision (Chen et al., 2011). Data are colored by the reacted concentration of β-caryophyllene.

Figure 7b omits a data set of Hoffmann et al. (1997) because the M_{org} exceeds the abscissa scale of the figure. For atmospheric conditions, ozonolysis rather than photooxidation is the dominant degradation pathway of β-caryophyllene (Atkinson and Arey, 2003).

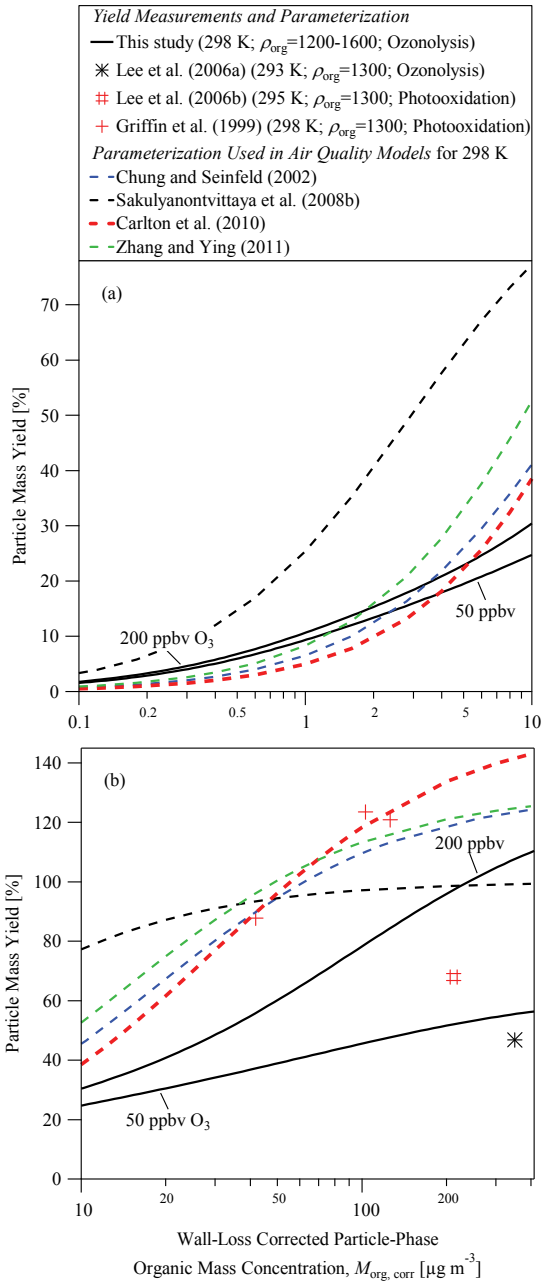

Fig. 7. Comparison of particle mass yields parameterized in this study to those reported in the literature for β-caryophyllene oxidation. Panel **(a)** shows the data in the atmospherically relevant range of organic particle mass concentration (0.1–10 µg m^{-3}). Panel **(b)** shows the data over an extended range of organic particle mass concentration (10–400 µg m^{-3}). A material density ρ_{org} of 1300 kg m^{-3} was assumed to convert the volume-based data sets of Lee et al. (2006a) and Griffin et al. (1999) to mass-based data sets. This density corresponded to $M_{org,corr} > 10$ µg m^{-3} of the present study (Fig. S3). A vaporization enthalpy of 40 kJ mol^{-1} was used for temperature compensation from 308 K to 298 K for the data reported by Griffin et al. (1999). The dashed lines show four different parameterizations that have been used in air quality and climate models.

4 Conclusions

This study investigated the role of second-generation products in the particle mass yield of β-caryophyllene ozonolysis. For concentrations that overlapped with those of the atmosphere (i.e., 0.1 to 10 $\mu g\,m^{-3}$, Chen et al., 2009; Slowik et al., 2010), the particle mass yield increases from 2 to 30 %. The yield is not sensitive to the ozone concentration. The explanation is that for this range of mass concentration there is a dominant contribution of low-volatility, fast-forming second-generation products to the particle phase. The O:C elemental ratio of 0.5 indicates that these low-volatility products have 7 to 8 oxygen atoms with estimated vapor pressures of 10^{-12} to 10^{-14} Pa (Li et al., 2011). The data further show that organic particle mass concentration inversely correlates with the oxidation state and the material density of the particle-phase organic material. Across the studied range of organic particle mass concentration (0.5–230 $\mu g\,m^{-3}$), the O:C ratio drops from 0.5 to 0.3, corresponding to a decrease in $\overline{OS}_c$ from -0.5 to -0.8. Material density likewise decreases from 1600 to 1300 $kg\,m^{-3}$, corresponding to the decreases in relative oxygen content.

Prior to the present study, no data points for the particle mass yield of β-caryophyllene ozonolysis were available in the atmospheric limit of $M_{org} < 10\,\mu g\,m^{-3}$. In the absence of data, regional and global chemical transport models have instead widely employed extrapolations of the data reported by Griffin et al. (1999) to estimate the contribution of sesquiterpene β-caryophyllene oxidation to atmospheric particle mass concentrations (Chung and Seinfeld, 2002; Sakulyanontvittaya et al., 2008b; Zhang and Ying, 2011) (details are provided in the Sect. C and Table S2 of the Supplement). Because the data reported by Griffin et al. (1999) were collected at 308 K and were volume-based, corrections were needed for model applications typically developed for 298 K. The corrections required estimates of the enthalpy of vaporization ΔH_{vap} and of material density. Different air-quality applications have used different estimates of these quantities, and as a result the parameterizations of mass yield have been different in various models, as represented by the dashed lines in Fig. 7. Using an updated ΔH_{vap} of 40 $kJ\,mol^{-1}$ as well as a material density ρ_{org} of 1300 $kg\,m^{-3}$ (Bahreini et al., 2005; Offenberg et al., 2006), Carlton et al. (2010) present the state-of-the-art parameterization. The comparison between our data set and the parameterization of Carlton et al. (2010) suggests a possible underestimate by that parameterization of 100 % to 300 % for organic particle mass concentrations less than 3 $\mu g\,m^{-3}$ given that ozonolysis rather than photooxidation is the dominant degradation pathway of β-caryophyllene. The difference could be in the underlying chemistry, keeping in mind that the parameterization is based on the photooxidation data set of Griffin et al. (1999) whereas the data of this study correspond to ozonolysis experiments.

The ultimate particle mass yield of β-caryophyllene ozonolysis was parameterized for the present study by mass-based stoichiometric yields $\alpha_0 = 0.17 \pm 0.05$, $\alpha_1 = 0.11 \pm 0.17$, and $\alpha_2 = 1.03 \pm 0.30$ for corresponding saturation concentrations of 1, 10, and 100 $\mu g\,m^{-3}$. Terms α_0 and α_1 had low sensitivity to ozone exposure for the investigated range of conditions whereas term α_2 increased from 0.32 ± 0.13 to 1.03 ± 0.30 as ozone exposure was increased. These findings potentially allow for simplified yet accurate parameterizations in air quality and climate models that seek to represent the ozonolysis particle mass yield of certain classes of biogenic compounds. The influence of additional important reaction conditions, such as NO_x concentrations, photolysis pathways, and particle aging, needs to be investigated in the future.

Supplementary material related to this article is available online at: http://www.atmos-chem-phys.net/12/3165/2012/acp-12-3165-2012-supplement.pdf.

Acknowledgements. This material is based upon work supported by the Office of Science (BES), US Department of Energy, Grant No. DE-FG02-08ER64529. Q. C. acknowledges support from the NASA Earth and Space Science Fellowship. Y. J. L. acknowledges support from the Hong Kong University of Science and Technology Overseas Research Award and the Research Grants Council of the Hong Kong Special Administrative Region, China (Project No. 610909). M. K. acknowledges support from the Japan Society for the Promotion of Science Postdoctoral Fellowship. The authors thank Amanda Mifflin and Mackenzie Smith for their assistance with the experiments. The authors thank Adam Bateman and Soeren Zorn for helpful discussion.

Edited by: H. Saathoff

References

Aiken, A. C., DeCarlo, P. F., and Jimenez, J. L.: Elemental analysis of organic species with electron ionization high-resolution mass spectrometry, Anal. Chem., 79, 8350–8358, doi:10.1021/ac071150w, 2007.

Aiken, A. C., Decarlo, P. F., Kroll, J. H., Worsnop, D. R., Huffman, J. A., Docherty, K. S., Ulbrich, I. M., Mohr, C., Kimmel, J. R., Sueper, D., Sun, Y., Zhang, Q., Trimborn, A., Northway, M., Ziemann, P. J., Canagaratna, M. R., Onasch, T. B., Alfarra, M. R., Prevot, A. S. H., Dommen, J., Duplissy, J., Metzger, A., Baltensperger, U., and Jimenez, J. L.: O/C and OM/OC ratios of primary, secondary, and ambient organic aerosols with high-resolution time-of-flight aerosol mass spectrometry, Environ. Sci. Technol., 42, 4478–4485, doi:10.1021/es703009q, 2008.

Alfarra, M. R., Coe, H., Allan, J. D., Bower, K. N., Boudries, H., Canagaratna, M. R., Jimenez, J. L., Jayne, J. T., Garforth, A. A., Li, S. M., and Worsnop, D. R.: Characterization of urban and rural organic particulate in the lower Fraser valley using two aerodyne aerosol mass spectrometers, Atmos. Environ., 38, 5745–5758, doi:10.1016/j.atmosenv.2004.01.054, 2004.

Atkinson, R. and Arey, J.: Gas-phase tropospheric chemistry of biogenic volatile organic compounds: a review, Atmos. Environ., 37, S197–S219, doi:10.1016/s1352-2310(03)00391-1, 2003.

Bahreini, R., Keywood, M. D., Ng, N. L., Varutbangkul, V., Gao, S., Flagan, R. C., Seinfeld, J. H., Worsnop, D. R., and Jimenez, J. L.: Measurements of secondary organic aerosol from oxidation of cycloalkenes, terpenes, and m-xylene using an Aerodyne aerosol mass spectrometer, Environ. Sci. Technol., 39, 5674–5688, doi:10.1021/es048061a, 2005.

Carlton, A. G., Bhave, P. V., Napelenok, S. L., Edney, E. D., Sarwar, G., Pinder, R. W., Pouliot, G. A., and Houyoux, M.: Model Representation of Secondary Organic Aerosol in CMAQv4.7, Environ. Sci. Technol., 44, 8553–8560, doi:10.1021/es100636q, 2010.

Chan, A. W. H., Kroll, J. H., Ng, N. L., and Seinfeld, J. H.: Kinetic modeling of secondary organic aerosol formation: effects of particle- and gas-phase reactions of semivolatile products, Atmos. Chem. Phys., 7, 4135–4147, doi:10.5194/acp-7-4135-2007, 2007.

Chan, M. N., Surratt, J. D., Chan, A. W. H., Schilling, K., Offenberg, J. H., Lewandowski, M., Edney, E. O., Kleindienst, T. E., Jaoui, M., Edgerton, E. S., Tanner, R. L., Shaw, S. L., Zheng, M., Knipping, E. M., and Seinfeld, J. H.: Influence of aerosol acidity on the chemical composition of secondary organic aerosol from beta-caryophyllene, Atmos. Chem. Phys., 11, 1735–1751, doi:10.5194/acp-11-1735-2011, 2011.

Chen, Q., Farmer, D. K., Schneider, J., Zorn, S. R., Heald, C. L., Karl, T. G., Guenther, A., Allan, J. D., Robinson, N., Coe, H., Kimmel, J. R., Pauliquevis, T., Borrmann, S., Poschl, U., Andreae, M. O., Artaxo, P., Jimenez, J. L., and Martin, S. T.: Mass spectral characterization of submicron biogenic organic particles in the Amazon Basin, Geophys. Res. Lett., 36, L20806, doi:10.1029/2009gl039880, 2009.

Chen, Q., Liu, Y., Donahue, N. M., Shilling, J. E., and Martin, S. T.: Particle-phase chemistry of secondary organic material: Modeled compared to measured O:C and H:C elemental ratios provide constraints, Environ. Sci. Technol., 45, 4763–4770, doi:10.1021/es104398s, 2011.

Chung, S. H. and Seinfeld, J. H.: Global distribution and climate forcing of carbonaceous aerosols, J. Geophys. Res., 107, 4407, doi:10.1029/2001jd001397, 2002.

DeCarlo, P. F., Slowik, J. G., Worsnop, D. R., Davidovits, P., and Jimenez, J. L.: Particle morphology and density characterization by combined mobility and aerodynamic diameter measurements, Part 1: Theory, Aerosol Sci. Technol., 38, 1185–1205, doi:10.1080/027868290903907, 2004.

DeCarlo, P. F., Kimmel, J. R., Trimborn, A., Northway, M. J., Jayne, J. T., Aiken, A. C., Gonin, M., Fuhrer, K., Horvath, T., Docherty, K. S., Worsnop, D. R., and Jimenez, J. L.: Field-deployable, high-resolution, time-of-flight aerosol mass spectrometer, Anal. Chem., 78, 8281–8289, doi:10.1021/ac061249n, 2006.

Donahue, N. M., Robinson, A. L., Stanier, C. O., and Pandis, S. N.: Coupled partitioning, dilution, and chemical aging of semivolatile organics, Environ. Sci. Technol., 40, 02635–02643, doi:10.1021/es052297c, 2006.

Ehara, K., Hagwood, C., and Coakley, K. J.: Novel method to classify aerosol particles according to their mass-to-charge ratio – Aerosol particle mass analyser, J. Aerosol Sci., 27, 217–234, 1996.

Fiore, A., Jacob, D. J., Liu, H., Yantosca, R. M., Fairlie, T. D., and Li, Q.: Variability in surface ozone background over the United States: Implications for air quality policy, J. Geophys. Res., 108, 4787, doi:10.1029/2003jd003855, 2003.

Fu, P. Q., Kawamura, K., Chen, J., and Barrie, L. A.: Isoprene, monoterpene, and sesquiterpene oxidation products in the high arctic aerosols during late winter to early summer, Environ. Sci. Technol., 43, 4022–4028, doi:10.1021/es803669a, 2009.

Griffin, R. J., Cocker, D. R., Flagan, R. C., and Seinfeld, J. H.: Organic aerosol formation from the oxidation of biogenic hydrocarbons, J. Geophys. Res., 104, 3555–3567, 1999.

Grosjean, D., Williams, E. L., Grosjean, E., Andino, J. M., and Seinfeld, J. H.: Atmospheric oxidation of biogenic hydrocarbons: Reaction of ozone with β-pinene, d-limonene, and trans-caryophyllene, Environ. Sci. Technol., 27, 2754–2758, 1993.

Helmig, D., Balsley, B., Davis, K., Kuck, L. R., Jensen, M., Bognar, J., Smith, T., Arrieta, R. V., Rodriguez, R., and Birks, J. W.: Vertical profiling and determination of landscape fluxes of biogenic nonmethane hydrocarbons within the planetary boundary layer in the Peruvian Amazon, J. Geophys. Res., 103, 25519–25532, doi:10.1029/98JD01023, 1998.

Helmig, D., Ortega, J., Duhl, T., Tanner, D., Guenther, A., Harley, P., Wiedinmyer, C., Milford, J., and Sakulyanontvittaya, T.: Sesquiterpene emissions from pine trees – Identifications, emission rates and flux estimates for the contiguous United States, Environ. Sci. Technol., 41, 1545–1553, doi:10.1021/es0618907, 2007.

Hoffmann, T., Odum, J. R., Bowman, F., Collins, D., Klockow, D., Flagan, R. C., and Seinfeld, J. H.: Formation of organic aerosols from the oxidation of biogenic hydrocarbons, J. Atmos. Chem., 26, 189–222, 1997.

Hu, D., Bian, Q., Li, T. W. Y., Lau, A. K. H., and Yu, J. Z.: Contributions of isoprene, monoterpenes, β-caryophyllene, and toluene to secondary organic aerosols in Hong Kong during the summer of 2006, J. Geophys. Res., 113, D22206, doi:10.1029/2008jd010437, 2008.

Jaoui, M. and Kamens, R. M.: Gas and particulate products distribution from the photooxidation of α-humulene in the presence of NO_x, natural atmospheric air and sunlight, J. Atmos. Chem., 46, 29–54, 2003.

Jaoui, M., Leungsakul, S., and Kamens, R. M.: Gas and particle products distribution from the reaction of β-caryophyllene with ozone, J. Atmos. Chem., 45, 261–287, 2003.

Jaoui, M., Lewandowski, M., Kleindienst, T. E., Offenberg, J. H., and Edney, E. O.: β-caryophyllinic acid: An atmospheric tracer for β-caryophyllene secondary organic aerosol, Geophys. Res. Lett., 34, L05816, doi:10.1029/2006gl028827, 2007.

Kanawati, B., Herrmann, F., Joniec, S., Winterhalter, R., and Moortgat, G. K.: Mass spectrometric characterization of β-caryophyllene ozonolysis products in the aerosol studied using an electrospray triple quadrupole and time-of-flight analyzer hybrid system and density functional theory, Rapid Commun. Mass Spectrom., 22, 165–186, 2008.

Katrib, Y., Martin, S. T., Rudich, Y., Davidovits, P., Jayne, J. T., and Worsnop, D. R.: Density changes of aerosol particles as a result of chemical reaction, Atmos. Chem. Phys., 5, 275–291, doi:10.5194/acp-5-275-2005, 2005.

King, S. M., Rosenoern, T., Shilling, J. E., Chen, Q., and Martin, S. T.: Cloud condensation nucleus activity of secondary organic

aerosol particles mixed with sulfate, Geophys. Res. Lett., 34, L24806, doi:10.1029/2007gl030390, 2007.

King, S. M., Rosenoern, T., Shilling, J. E., Chen, Q., and Martin, S. T.: Increased cloud activation potential of secondary organic aerosol for atmospheric mass loadings, Atmos. Chem. Phys., 9, 2959–2971, doi:10.5194/acp-9-2959-2009, 2009.

Kleindienst, T. E., Smith, D. F., Li, W., Edney, E. O., Driscoll, D. J., Speer, R. E., and Weathers, W. S.: Secondary organic aerosol formation from the oxidation of aromatic hydrocarbons in the presence of dry submicron ammonium sulfate aerosol, Atmos. Environ., 33, 3669–3681, 1999.

Kleindienst, T. E., Jaoui, M., Lewandowski, M., Offenberg, J. H., Lewis, C. W., Bhave, P. V., and Edney, E. O.: Estimates of the contributions of biogenic and anthropogenic hydrocarbons to secondary organic aerosol at a southeastern US location, Atmos. Environ., 41, 8288–8300, doi:10.1016/j.atmosenv.2007.06.045, 2007.

Knutson, E. O. and Whitby, K. T.: Aerosol classification by electric mobility: Apparatus, theory, and applications, J. Aerosol Sci., 6, 443–451, 1975.

Kroll, J. H., Donahue, N. M., Jimenez, J. L., Kessler, S. H., Canagaratna, M. R., Wilson, K. R., Altieri, K. E., R.Mazzoleni, L., Wozniak, A. S., Bluhm, H., Mysak, E. R., Smith, J. D., Kolb, C. E., and Worsnop, D. R.: Carbon oxidation state as a metric for describing the chemistry of atmospheric organic aerosol, Nature Chem., 3, 133–139, doi:10.1038/nchem.948, 2011.

Kuwata, M., Zorn, S. R., and Martin, S. T.: Using elemental ratios to predict the density of organic material composed of carbon, hydrogen, and oxygen, Environ. Sci. Technol., 46, 787–794, doi:10.1021/es202525q, 2012.

Lee, A., Goldstein, A. H., Keywood, M. D., Gao, S., Varutbangkul, V., Bahreini, R., Ng, N. L., Flagan, R. C., and Seinfeld, J. H.: Gas-phase products and secondary aerosol yields from the ozonolysis of ten different terpenes, J. Geophys. Res., 111, D07302, doi:10.1029/2005jd006437, 2006a.

Lee, A., Goldstein, A. H., Kroll, J. H., Ng, N. L., Varutbangkul, V., Flagan, R. C., and Seinfeld, J. H.: Gas-phase products and secondary aerosol yields from the photooxidation of 16 different terpenes, J. Geophys. Res., 111, D17305, doi:10.1029/2006jd007050, 2006b.

Li, Y. J., Chen, Q., Guzman, M. I., Chan, C. K., and Martin, S. T.: Second-generation products contribute substantially to the particle-phase organic material produced by β-caryophyllene ozonolysis, Atmos. Chem. Phys., 11, 121–132, doi:10.5194/acp-10-1-2010, 2011.

Liu, B. Y. H. and Lee, K. W.: An aerosol generator of high stability, Am. Ind. Hyg. Assoc. J., 36, 861–865, doi:10.1080/0002889758507357, 1975.

Matsunaga, A. and Ziemann, P. J.: Gas-wall partitioning of organic compounds in a Teflon film chamber and potential effects on reaction product and aerosol yield measurements, Aerosol Sci. Technol., 44, 881–892, doi:10.1080/02786826.2010.501044, 2010.

Matthew, B. M., Middlebrook, A. M., and Onasch, T. B.: Collection efficiencies in an Aerodyne Aerosol Mass Spectrometer as a function of particle phase for laboratory generated aerosols, Aerosol Sci. Technol., 42, 884–898, doi:10.1080/02786820802356797, 2008.

McMurry, P. H. and Grosjean, D.: Gas and aerosol wall losses in Teflon film smog chambers, Environ. Sci. Technol., 19, 1176–1182, 1985.

McMurry, P. H. and Rader, D. J.: Aerosol wall losses in electrically charged chambers, Aerosol Sci. Technol., 4, 249–268, 1985.

Mensah, A. A., Buchholz, A., Mentel, T. F., Tillmann, R., and Kiendler-Scharr, A.: Aerosol mass spectrometric measurements of stable crystal hydrates of oxalates and inferred relative ionization efficiency of water, J. Aerosol Sci., 42, 11–19, doi:10.1016/j.jaerosci.2010.10.003, 2011.

Neue, U. D., Kele, M., Bunner, B., Kromidas, A., Dourdeville, T., Mazzeo, J. R., Grumbach, E. S., Serpa, S., Wheat, T. E., Hong, P., and Gilar, M.: Ultra-Performance Liquid Chromatography Technology and Applications, in: Adv. Chromatogr. (Boca Raton, FL, U. S.), edited by: Grushka, E., and Grinberg, N., Advances in Chromatography, 99–143, 2010.

Ng, N. L., Kroll, J. H., Keywood, M. D., Bahreini, R., Varutbangkul, V., Flagan, R. C., Seinfeld, J. H., Lee, A., and Goldstein, A. H.: Contribution of first- versus second-generation products to secondary organic aerosols formed in the oxidation of biogenic hydrocarbons, Environ. Sci. Technol., 40, 2283–2297, doi:10.1021/es052269u, 2006.

Ng, N. L., Chhabra, P. S., Chan, A. W. H., Surratt, J. D., Kroll, J. H., Kwan, A. J., McCabe, D. C., Wennberg, P. O., Sorooshian, A., Murphy, S. M., Dalleska, N. F., Flagan, R. C., and Seinfeld, J. H.: Effect of NO_x level on secondary organic aerosol (SOA) formation from the photooxidation of terpenes, Atmos. Chem. Phys., 7, 5159–5174, doi:10.5194/acp-7-5159-2007, 2007.

Nguyen, T. L., Winterhalter, R., Moortgat, G., Kanawati, B., Peeters, J., and Vereecken, L.: The gas-phase ozonolysis of β-caryophyllene ($C_{15}H_{24}$). Part II: A theoretical study, Phys. Chem. Chem. Phys., 11, 4173–4183, 2009.

Odum, J. R., Hoffmann, T., Bowman, F., Collins, D., Flagan, R. C., and Seinfeld, J. H.: Gas/particle partitioning and secondary organic aerosol yields, Environ. Sci. Technol., 30, 2580–2585, 1996.

Offenberg, J. H., Kleindienst, T. E., Jaoui, M., Lewandowski, M., and Edney, E. O.: Thermal properties of secondary organic aerosols, Geophys. Res. Lett., 33, L03816, doi:10.1029/2005gl024623, 2006.

Offenberg, J. H., Lewandowski, M., Edney, E. O., Kleindienst, T. E., and Jaoui, M.: Influence of aerosol acidity on the formation of secondary organic aerosol from biogenic precursor hydrocarbons, Environ. Sci. Technol., 43, 7742–7747, doi:10.1021/es901538e, 2009.

Pankow, J. F.: An absorption-model of gas-particle partitioning of organic compounds in the atmosphere, Atmos. Environ., 28, 185–188, 1994a.

Pankow, J. F.: An absorption-model of the gas aerosol partitioning involved in the formation of secondary organic aerosol, Atmos. Environ., 28, 189–193, 1994b.

Pankow, J. F. and Asher, W. E.: SIMPOL.1: a simple group contribution method for predicting vapor pressures and enthalpies of vaporization of multifunctional organic compounds, Atmos. Chem. Phys., 8, 2773–2796, doi:10.5194/acp-8-2773-2008, 2008.

Pierce, J. R., Engelhart, G. J., Hildebrandt, L., Weitkamp, E. A., Pathak, R. K., Donahue, N. M., Robinson, A. L., Adams, P. J., and Pandis, S. N.: Constraining particle evolution from wall losses, coagulation, and condensation-evaporation in smog-

chamber experiments: Optimal estimation based on size distribution measurements, Aerosol Sci. Technol., 42, 1001–1015, doi:10.1080/02786820802389251, 2008.

Presto, A. A. and Donahue, N. M.: Investigation of α-pinene plus ozone secondary organic aerosol formation at low total aerosol mass, Environ. Sci. Technol., 40, 3536–3543, doi:10.1021/es052203z, 2006.

Sakulyanontvittaya, T., Duhl, T., Wiedinmyer, C., Helmig, D., Matsunaga, S., Potosnak, M., Milford, J., and Guenther, A.: Monoterpene and sesquiterpene emission estimates for the United States, Environ. Sci. Technol., 42, 1623–1629, doi:10.1021/es702274e, 2008a.

Sakulyanontvittaya, T., Guenther, A., Helmig, D., Milford, J., and Wiedinmyer, C.: Secondary organic aerosol from sesquiterpene and monoterpene emissions in the United States, Environ. Sci. Technol., 42, 8784–8790, doi:10.1021/es800817r, 2008b.

Seinfeld, J. H. and Pankow, J. F.: Organic atmospheric particulate material, Annu. Rev. Phys. Chem., 54, 121–140, doi:10.1146/annurev.physchem.54.011002.103756, 2003.

Seinfeld, J. H., Kleindienst, T. E., Edney, E. O., and Cohen, J. B.: Aerosol growth in a steady-state, continuous flow chamber: Application to studies of secondary aerosol formation, Aerosol Sci. Technol., 37, 728–734, doi:10.1080/02786820390214954, 2003.

Shilling, J. E., Chen, Q., King, S. M., Rosenoern, T., Kroll, J. H., Worsnop, D. R., McKinney, K. A., and Martin, S. T.: Particle mass yield in secondary organic aerosol formed by the dark ozonolysis of α-pinene, Atmos. Chem. Phys., 8, 2073–2088, doi:10.5194/acp-8-2073-2008, 2008.

Shilling, J. E., Chen, Q., King, S. M., Rosenoern, T., Kroll, J. H., Worsnop, D. R., DeCarlo, P. F., Aiken, A. C., Sueper, D., Jimenez, J. L., and Martin, S. T.: Loading-dependent elemental composition of α-pinene SOA particles, Atmos. Chem. Phys., 9, 771-782, doi:10.5194/acp-9-771-2009, 2009.

Shu, Y. H. and Atkinson, R.: Atmospheric lifetimes and fates of a series of sesquiterpenes, J. Geophys. Res., 100, 7275–7281, doi:10.1029/95JD00368, 1995.

Slowik, J. G., Stroud, C., Bottenheim, J. W., Brickell, P. C., Chang, R. Y.-W., Liggio, J., Makar, P. A., Martin, R. V., Moran, M. D., Shantz, N. C., Sjostedt, S. J., van Donkelaar, A., Vlasenko, A., Wiebe, H. A., Xia, A. G., Zhang, J., Leaitch, W. R., and Abbatt, J. P. D.: Characterization of a large biogenic secondary organic aerosol event from eastern Canadian forests, Atmos. Chem. Phys., 10, 2825–2845, doi:10.5194/acp-10-2825-2010, 2010.

Solomon, P., Cowling, E., Hidy, G., and Furiness, C.: Comparison of scientific findings from major ozone field studies in North America and Europe, Atmos. Environ., 34, 1885–1920, 2000.

Wang, S. C. and Flagan, R. C.: Scanning electrical mobility spectrometer, J. Aerosol Sci., 20, 1485–1488, doi:10.1016/0021-8502(89)90868-9, 1989.

Winterhalter, R., Herrmann, F., Kanawati, B., Nguyen, T. L., Peeters, J., Vereecken, L., and Moortgat, G. K.: The gas-phase ozonolysis of β-caryophyllene ($C_{15}H_{24}$). Part I: an experimental study, Phys. Chem. Chem. Phys., 11, 4152–4172, doi:10.1039/b817824k, 2009.

Zhang, H. L. and Ying, Q.: Secondary organic aerosol formation and source apportionment in Southeast Texas, Atmos. Environ., 45, 3217–3227, doi:10.1016/j.atmosenv.2011.03.046, 2011.